Marine Geophysical Researches **22:** 265–287, 2001.

Velocity-Interface Structure of the Southwestern Ryukyu Subduction Zone from EW9509-1 OBS/MCS Data

Tan K. Wang[1,*], Kirk McIntosh[2], Yosio Nakamura[2], Char-Shine Liu[3] and How-Wei Chen[4]
[1]*Institute of Applied Geophysics, National Taiwan Ocean University, Keelung, Taiwan, ROC;*
[2]*Institute for Geophysics, University of Texas, Austin, Texas, USA;*
[3]*Institute of Oceanography, National Taiwan University, Taipei, Taiwan, ROC;*
[4]*Institute of Applied Geophysics, National Chung Cheng University, Chiayi, Taiwan, ROC;*
[*]*Author for correspondence (Fax: 886-2-24625038; E-mail: tkwang@mail.ntou.edu.tw)*

Key words: OBS, crustal structure, subduction, ray, travel-time inversion

Abstract

A wide-angle seismic survey, combining ocean-bottom seismometers (OBS) and multi-channel seismic (MCS) profiling, was implemented in the southwestern Ryukyu subduction zone during August and September 1995. In this paper, we present the data analysis of eight OBSs and the corresponding MCS line along profile EW9509-1 from this experiment. Seismic data modeling includes identification of refracted and reflected arrivals, initial model building from velocity analysis of the MCS data, and simultaneous and layer-stripping inversions of the OBS and MCS arrivals. The velocity-interface structure constructed along profile EW9509-1 shows that the northward subduction of the Philippine Sea Plate has resulted in a northward thickening of the sediments of the Ryukyu Trench and the Yaeyama accretionary wedge north of the trench. The boundary between the subducting oceanic crust and the overriding continental crust (represented by a velocity contour of 6.75 km/s) and a sudden increase of the subducting angle (from 5 degrees to 25 degrees) are well imaged below the Nanao Basin. Furthermore, velocity undulation and interface variation are found within the upper crust of the Ryukyu Arc. Therefore, the strongest compression due to subduction and a break-off of the slab may have occurred and induced the high seismicity in the forearc region.

Introduction

Crustal structures imaged by ocean-bottom seismometer (OBS) data using air-gun sources generally fill gaps between shallow structures obtained from multi-channel seismic (MCS) profiles and deeper structures obtained using earthquake seismology in the marine environment. Several OBS surveys in the northeastern, middle and southwestern Ryukyu subduction zones were successfully implemented for imaging of the crustal structures in 1984, 1988 and 1985/1995, respectively (Figure 1). An OBS velocity model of 1984-2 (Iwasaki et al., 1990) shows that the subducting angle changes from about 5 degrees to 10 degrees below the southeastern part of the sedimentary wedge in the northeastern Ryukyu subduction zone. It was also found that the continental crust at the collision front is deformed and dragged down by subduction of the oceanic crust. On the other hand, the subducting angle in an OBS velocity model of 1988-2A in the middle Ryukyu subduction zone is uniform and about 5 degrees (Kodaira et al., 1996). The first OBS survey in the southwestern subduction zone was conducted in 1985 by Hagen et al. (1988). Their results illustrated the northward subduction of the PSP beneath the Ryukyu Arc but were not well constrained in the lower crust. Although OBS data acquired in the Ryukyu Arc have provided reliable P-wave velocity models of the crustal structures, the intra-crustal interfaces and the sedimentary structures could not be well imaged due to weak air-gun shots, insufficient trace spacing and a lack of combined MCS data in the experiments.

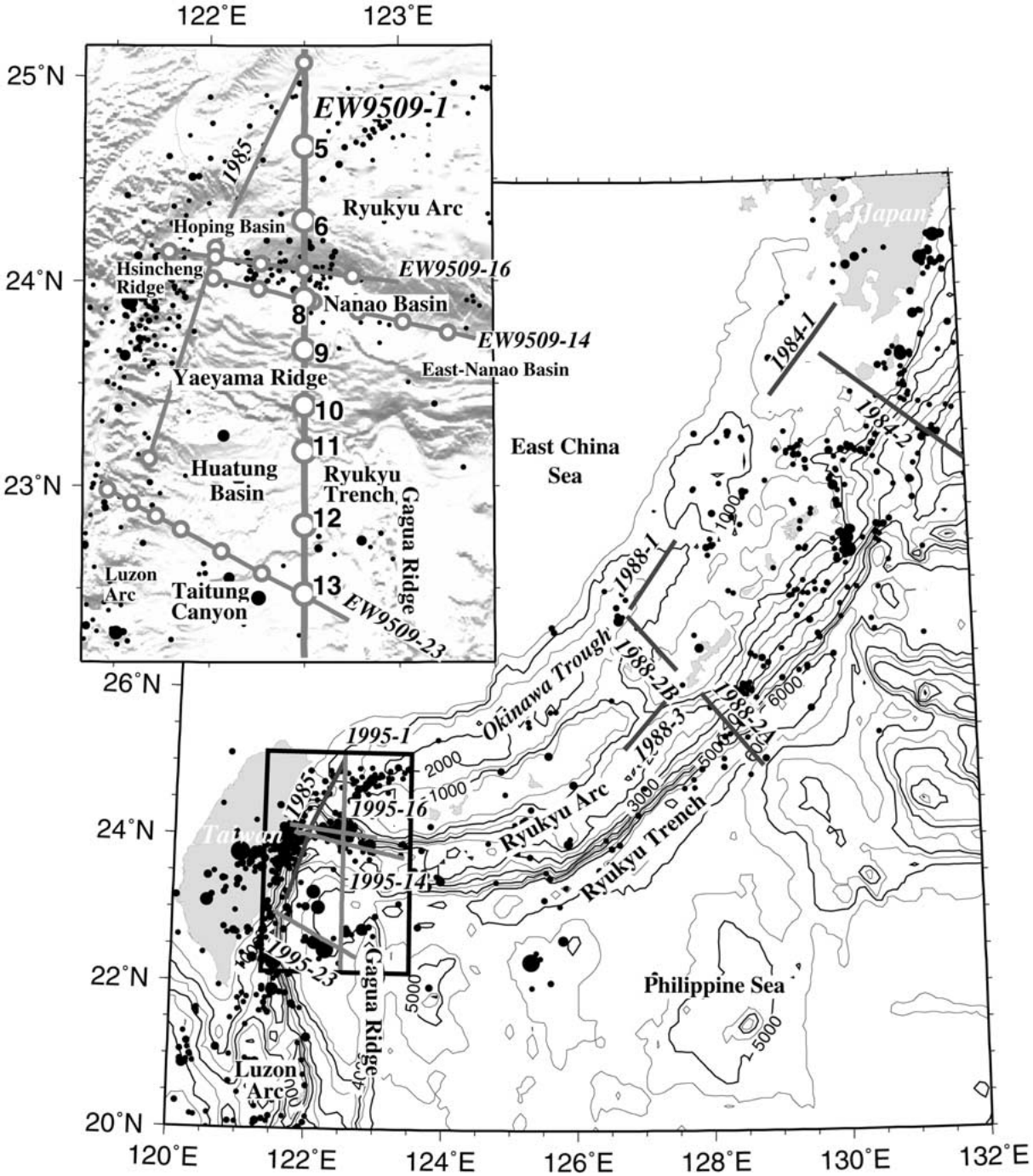

Figure 1. OBS lines, teleseismically determined epicenters (CNSS catalogue), bathymetry and tectonic features in the Ryukyu subduction zone. Two OBS surveys of the southwestern Ryukyu Arc was conducted in 1985 and 1995 within the area inside the black frame, enlarged in the illuminated bathymetry (Liu et al., 1998) in the upper left corner. Other OBS experiments in the middle (Kodaira et al., 1996) and northeastern (Iwasaki et al., 1990) Ryukyu Arcs are denoted by the years, 1988 and 1984, respectively, in which they were conducted. The contour interval of bathymetry is 500 m. In the inset, the OBS stations and the OBS/MCS lines are indicated by open circles and solid lines, respectively. In particular, only the EW9509-1 seismic line (thicker) with eight OBSs (open circles) is investigated in this study.

Using a large air-gun array and incorporating MCS data, three profiles of the OBS data (EW9509-14, EW9509-16 and EW9509-23) were acquired in the southwestern Ryukyu subduction zone (Figure 1). An OBS velocity model of EW9509-14 (McIntosh and Nakamura, 1998) shows that the thickness of the Ryukyu Arc basement (velocity $>$ 5 km/s) and the subducting Philippine Sea Plate (PSP) below the Nanao Basin (intersection with EW9509-1) are 10∼12 km and 8∼12 km, respectively. Results from modeling the OBS data of profile EW9509-16 (Wang and Chiang, 1998) suggest that the thickness of the Ryukyu Arc basement (5.5∼6.75 km/s) and the subducting PSP crust (6.75∼7.75 km/s) are 10∼15 km and 8∼12 km, respectively. An OBS velocity model of EW9509-23 (Yang and Wang, 1998) off southeastern Taiwan shows that the thickness of the oceanic crust (4.5∼7.75 km/s) southeast of OBS station 31 is 5∼7 km. Northwest of OBS station 31, the crust thickens northwestward.

The previous results of OBS data modeling in the Ryukyu subduction zone have lacked sufficient constraints on the structural interfaces from the reflected arrivals of seismic data. In this paper, we present travel-time modeling (Zelt, 1999) of an EW9509-1 MCS/OBS profile parallel to the subduction direction. This modeling approach includes identification of refracted and reflected arrivals, velocity analysis of the MCS data, simultaneous inversion of MCS arrivals and the individual phase in the OBS data, and minimum parameterization of the model grids.

Tectonic Setting

Ryukyu subduction system

The Ryukyu trench-arc-backarc system in the northwest Pacific is one of the most active convergent margins in the circum-Pacific belt. The Ryukyu Trench, with accumulated sediments and extending from Japan to Taiwan (Figure 1), is overlying the subducting PSP. The Ryukyu Arc is situated northwest of the trench and over-thrusts the PSP. Further northwest, a sedimentary basin of the Okinawa Trough has been formed by back-arc spreading between the East China Sea and the Ryukyu Arc (Kimura, 1985). Volcanic activity associated with the back-arc spreading has been found in the southern Okinawa Trough whereas active volcanoes in the Ryukyu Arc have occurred only in the northeastern part (Sibuet et al., 1987, 1998). In addition to these trench-arc-backarc structures, accretionary prism and forearc basins (Liu et al., 1997; Lallemand et al., 1999; Font et al., 2001) are lying between the trench and the arc where northwestward subduction of the PSP has started beneath the Eurasian Plate (EP).

The complexity of the southwestern Ryukyu subduction system investigated in this paper can be observed from the earthquake epicenters and the bathymetry. The epicenters, indicated by solid circles in Figure 1, are derived from the CNSS (Council of the National Seismic System) catalogue from 1963 onwards for magnitudes greater than 5 and depths less than 40 km in the Ryukyu subduction zone. These epicenters suggest that the most active subduction of the Ryukyu trench-arc-backarc system for both oceanic and continental crusts (depth less than 40 km) is located underneath the southwestern Ryukyu Arc. West of 123° E, the bathymetric trend of the Ryukyu arc-trench system gradually turns northward to a NW-SE direction in close proximity to the Taiwan (Figure 1). Hence, the crustal structures in the southwestern part of the Ryukyu subduction zone are complex and different from those of the northeastern and middle Ryukyu Arcs (Iwasaki et al., 1990; Kodaira et al., 1996).

Southwestern Ryukyu subduction system

Since the southwestern Ryukyu subduction system is terminated by the arc-continent collision of the Taiwan orogen between EP and PSP (Figure 1), tectonic structures in this area have also been affected by oblique plate convergence (Lallemand et al., 1999), arc-continent collision of present-day Taiwan (Huang et al., 2000) and/or arc-arc collision of paleo-Taiwan (Sibuet and Hsu, 1997). Collision between the Luzon Arc and the EP along the Coastal Range of Taiwan and collision between the Luzon Arc and the Ryukyu Arc below the forearc basins may have resulted in distinct bathymetries of the Hoping Basin, Hsincheng Ridge and Yaeyama Ridge (inset of Figure 1). South of the Ryukyu arc-trench system, the Huatung Basin lies between the Luzon Arc and the Gagua Ridge. Through investigation of deep seismic profiles, the Gagua Ridge was found to be northward subducting beneath the Ryukyu forearc region (Schnürle et al., 1998a).

Earthquake epicenters in the southwestern Ryukyu subduction zone (the solid circles in the inset of Figure 1) are distributed mainly in the southern Okinawa

Trough, the Nanao Basin, and the Coastal Range. To explain seismicity below the Nanao Basin, various types of tectonic faulting have been proposed. Lallemand et al. (1997) suggested a tear fault below the forearc basins to explain the northward subduction and the westward over-thrust of the PSP. Kao et al. (1998) proposed thrust faulting along the subducting interface based on an investigation of focal mechanisms beneath the Nanao Basin. From bathymetry and seismic reflection data, a right-lateral strike-slip fault developed on top of the Yaeyama accretionary prism was inferred from slip-partition of the oblique convergence in this area (Lallemand et al., 1999). This strike-slip fault may mark the southern boundary of the Ryukyu Arc basement (Font et al., 2001).

In this paper, we present an analysis of a N-S trending seismic line, EW9509-1, in the southwestern Ryukyu subduction system (Figure 1). The OBS/MCS data were analyzed to investigate the following important tectonic issues in this region. The first goal is to determine the crustal structures in order to understand the velocity variation within the Yaeyama accretionary wedge, the southward extension of the Ryukyu Arc basement, and the subduction boundary of the PSP and the Ryukyu Arc underneath the Yaeyama accretionary wedge. Another goal is to investigate the impact of plate convergence on earthquake faulting, e.g., reasons for the high seismicity below the Nanao Basin, as well as the location, depth, length and dipping angle of the active tectonic faulting.

OBS Data Acquisition and Processing

The MCS/OBS data used in this study were acquired in August and September 1995 during a Republic of China and US cooperative experiment for imaging crustal structures (Liu et al., 1997). In this experiment, 39 OBSs were deployed from the *R/V Ocean Researcher I* and received signals with shot spacing of about 40∼80 m from an air-gun array of 183 *l* on the *R/V Maurice Ewing*.

The vertical component of geophone data from eight OBSs and the data from corresponding MCS line of EW9509-1 are employed in this paper to construct the P-wave velocity model since the hydrophone data in this experiment is generally similar but less coherent than the vertical component of geophone data. From modeling two horizontal components of geophone data, Wang and Pan (2001) have also presented the crustal Poisson's ratio along EW9509-1. The EW9509-1 OBS/MCS line, extended from north to south for more than 300 km, covers the southern Okinawa Trough, Ryukyu Arc, Nanao Forearc Basin, Yaeyama Accretionary Ridge, Ryukyu Trench and Huatung Basin (inset of Figure 1). The velocity model of EW9509-1, also constrained by three other OBS profiles at their intersections, demonstrates how the oceanic crust subducts underneath the continental crust, and how the crustal structures relate to earthquake faulting.

Data processing prior to presentation and identification of the OBS arrivals includes station relocation, generation of formatted OBS data and signal enhancement. All components of the OBS data are considered to invert the location and the orientation of all stations. The incorporation of two horizontal components for determining the station orientation can also enhance the station relocation since water arrivals used in relocation come from a shooting line in 2D acquisition. Table 1 lists the longitude, latitude and depth of eight OBS stations along EW9509-1 computed using OBSTOOL (Christeson, 1995). The average errors of the location and the orientation for the eight stations are about 20 m and 15 degrees, respectively. OBS data sampled at intervals of 4 ms are subsequently formatted with a reduction velocity of 8 km/s and with a time span of 12 s. The maximum offset (−84410∼161211 m) and the number of traces (4019∼5724) recorded at the OBS stations (Table 1) vary from station to station because of irregular shot intervals of 10∼50 m caused by the strong and unsteady Kuroshio Current.

The strong previous shot noises in the OBS data (e.g., inclined noise bands with the same slope as the water waves shown in Figure 2) are due to the short shot interval of 20 s used for optimizing the MCS data acquisition. These noises are reduced by lining up traces according to the previous shot time, and by f-k filtering (W. S. Holbrook and E. C. Reiter, unpublished manuscript, 1992). Other signal enhancements, including band-pass filtering (over the range of 3–15 Hz at far offsets and 10–30 Hz at near offsets), scaling of abnormal amplitudes, and trace mixing of eight adjacent traces, are also applied to all the OBS data using the seismic processing software SIOSEIS (Henkart, 2000).

Table 1. OBS locations, maximum offsets and number of traces.

OBS station	OBS 13	OBS 12	OBS 11	OBS 10	OBS 9	OBS 8	OBS 6	OBS 5
Longitude (E)	122.49964	122.50081	122.5046	122.50385	122.49992	122.50158	122.49938	122.50127
Latitude (N)	22.47208	22.80522	23.17222	23.39893	23.6695	23.91581	24.29949	24.66324
Depth (m)	4923	5265	5643	4545	2900	3640	293	455
Max. offset[a] (m)	−36680 161211	−73571 156629	−79856 143975	−76665 138467	−79038 125773	−84410 108628	−62002 94710	−62390 54391
No. traces	4742	5611	5723	5716	5724	5711	5054	4019

[a]Negative/positive values indicate the offsets to the south/north

Phase Identification and Seismic Characteristics of OBS Records

Once the best presentation of the OBS data is obtained, we carry out arrival selection and phase identification. We first select the strong refracted arrivals (mostly from offsets less than 60 km) and clear reflected arrivals (mostly from sedimentary reflectors and wide-angle reflections). Later and weak arrivals (e.g., the white lines shown in Figures 3 to 6) are then selected iteratively by superimposing the calculated arrivals of the updated velocity-interface models on the OBS data (Zelt, 1999). Selection of these later arrivals is difficult because they are usually interfered with multiples, converted shear waves and out-of-plane signals. However, dense traces of the OBS data (average trace interval 40 m) and intensive efforts enable identification to be as complete as possible. In this study, most of the refracted and reflected arrivals from three sedimentary layers, three crustal layers and the upper mantle (Table 2) are identified by zooming into the local area with coherent signals and by using a trial-and-error approach. Uncertainty about these arrival selections is generally related to the signal to noise ratio and the frequency content. At near offsets or arrivals from shallow structures, the uncertainty of the selections is generally low, about 20∼50 ms, because the dominant frequency of the clear signal is about 25 Hz. However, at far offsets for deep levels when the dominant frequency is less than 10 Hz, the uncertainty of the selections can exceed 100 ms. In the following, we shall present the vertical component of the OBS data for both the entire section and its enlarged section. Trace amplitudes in the entire section of OBS data are scaled by multiplying with the absolute offset (|X|), while those in the enlarged section are generally adjusted for the sake of equal balancing among all the traces. In the following, phase identification and the seismic characteristics of the OBS data are presented for each geological province along the profile from south to north.

Huatung Basin

Reflected arrivals from the sedimentary interfaces were clearly recorded at OBS stations 12 and 13 in the Huatung Basin (e.g., Ps1P, Ps2P and Ps3P at offsets less than 10 km as shown in Figure 2). However, phase identification of the OBS arrivals from the sediment is not straightforward and will be more fully explained based on results of MCS data in the next section.

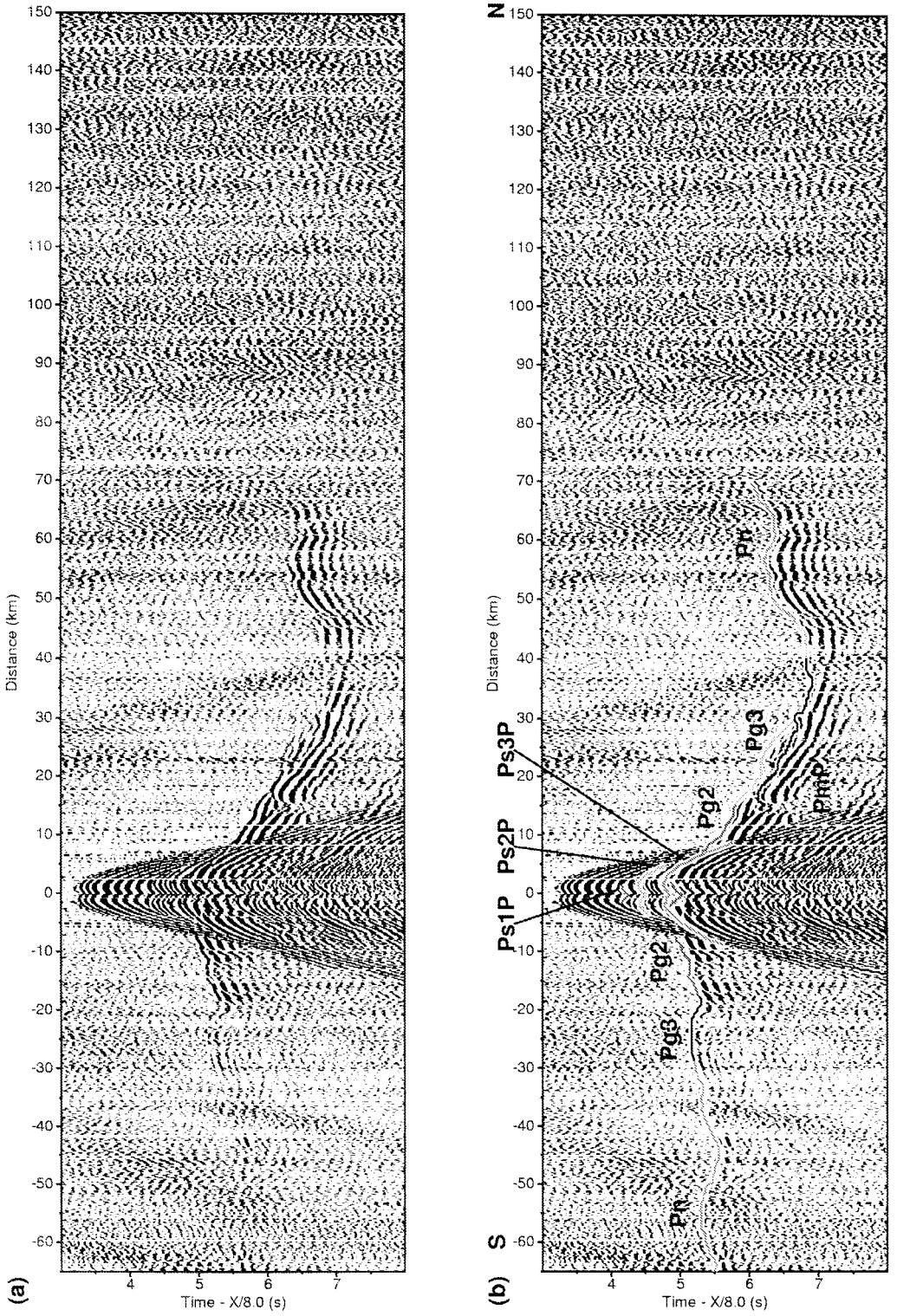

Figure 2. (a) Vertical component of the OBS data and (b) selected arrivals superimposed on the OBS data from station 12 in the Huatung Basin.

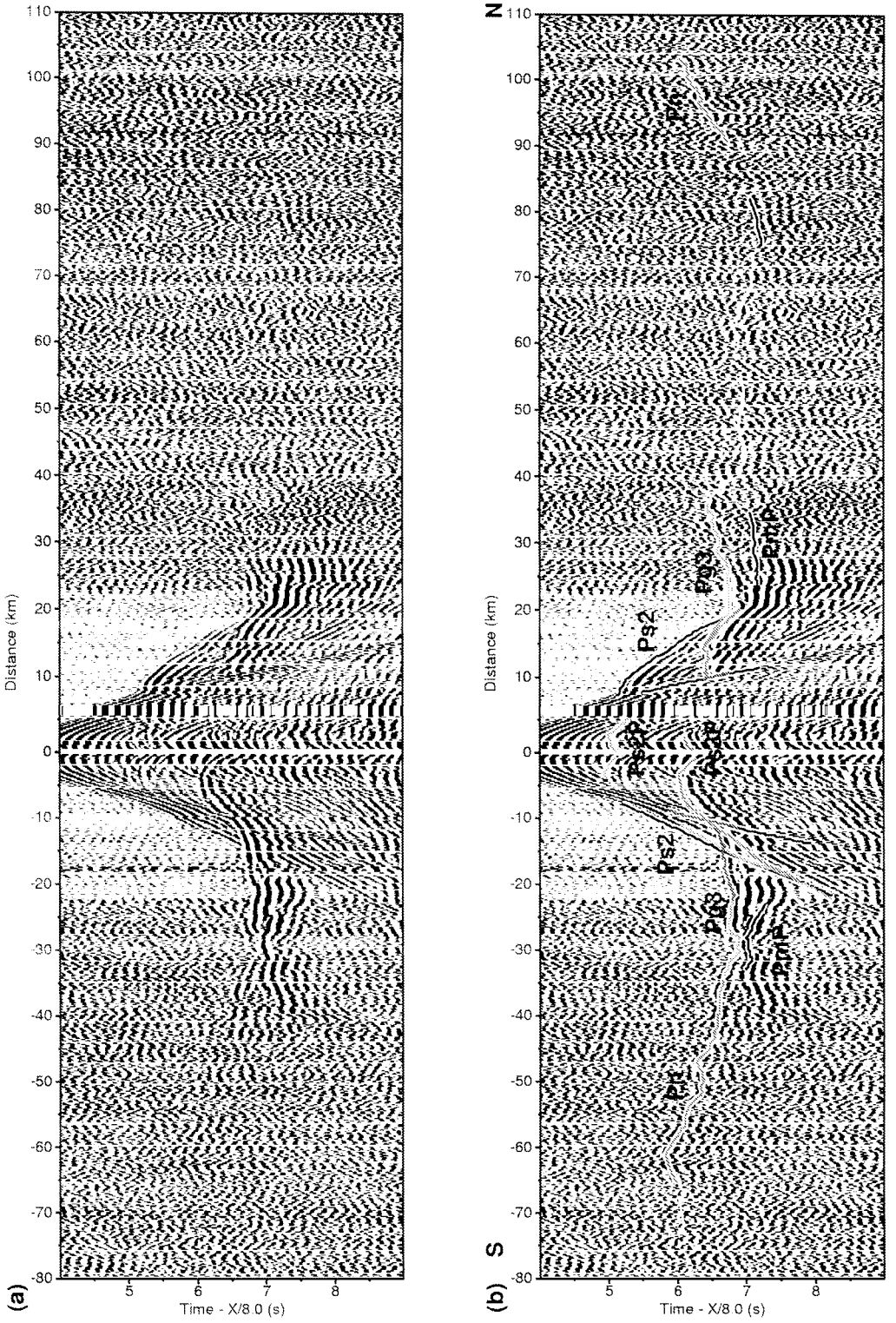

Figure 3. (a) Vertical component of the OBS data and (b) selected arrivals superimposed on the OBS data from station 11 in the Ryukyu Trench. Weak arrivals (white lines) are not used in inversion but are considered to demonstrate the ray coverage shown in Figure 9.

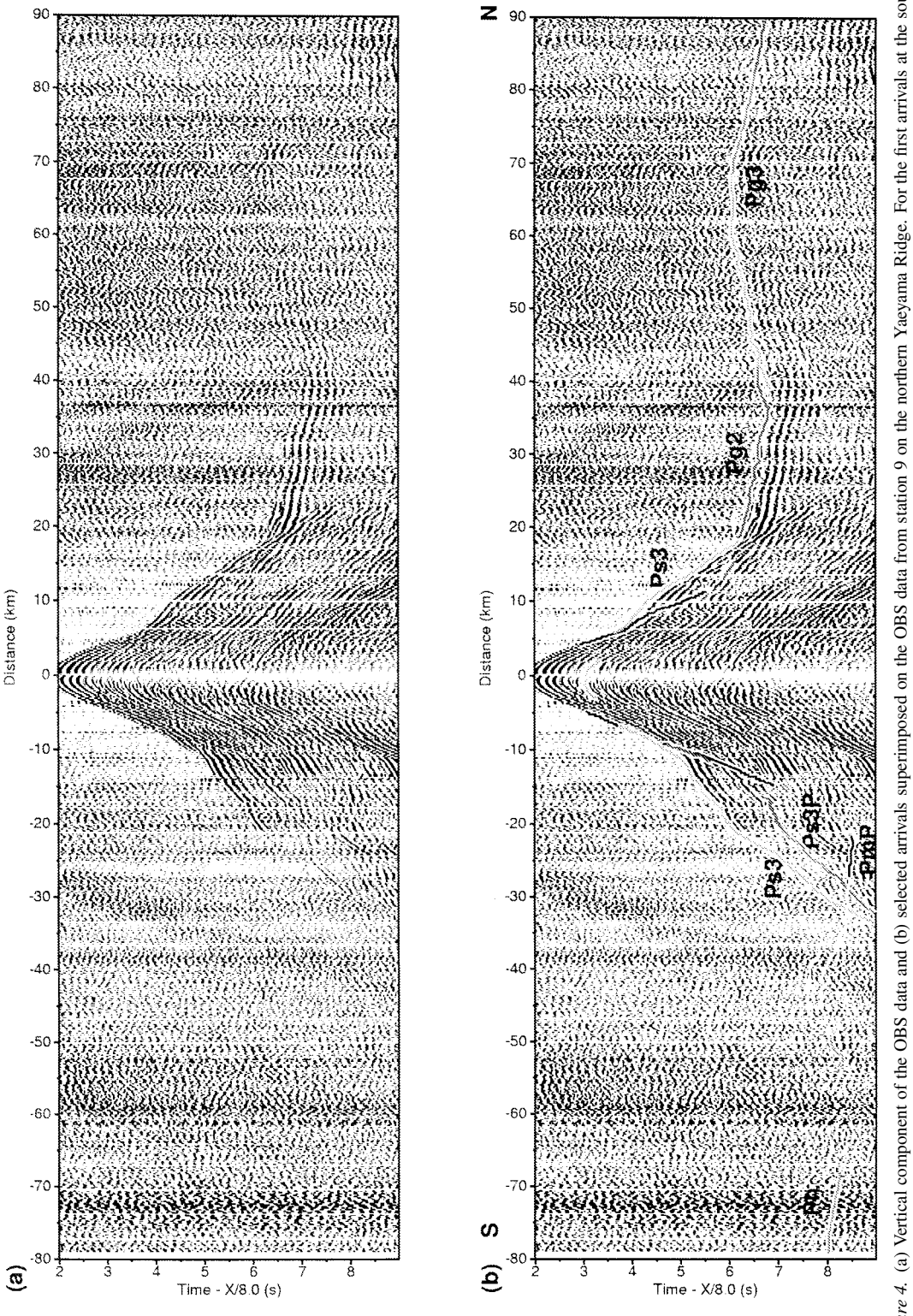

Figure 4. (a) Vertical component of the OBS data and (b) selected arrivals superimposed on the OBS data from station 9 on the northern Yaeyama Ridge. For the first arrivals at the southern far-offset, the upper-mantle refraction (Pn) can be observed, but the refraction through the crust is weak.

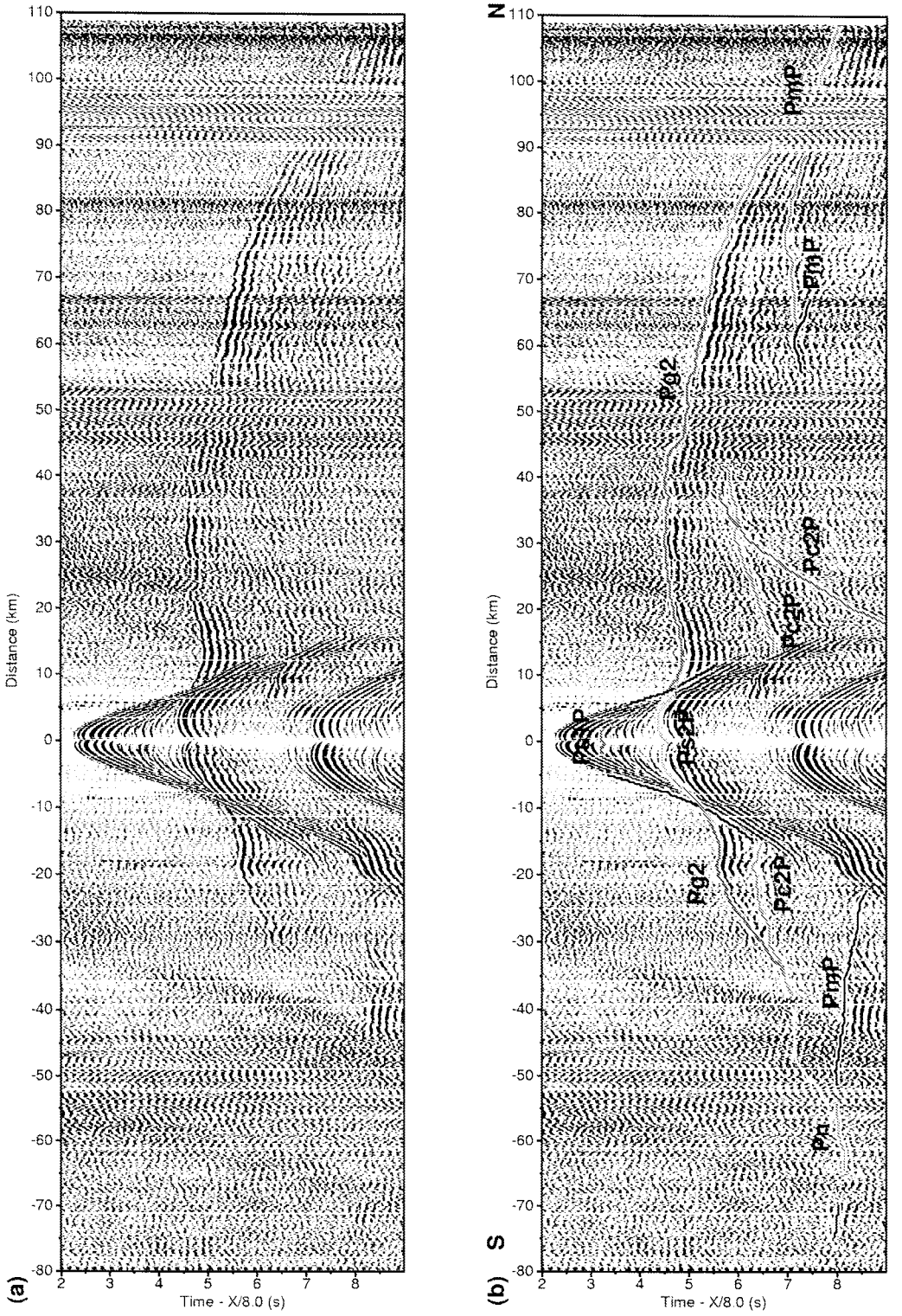

Figure 5. (a) Vertical component of the OBS data and (b) selected arrivals superimposed on the OBS data from station 8 in the Nanao Basin. OBS data of this station demonstrate that the high number of arrival picks may be due to its location in the sedimentary basin and above the thick upper crust where rays travel through more readily.

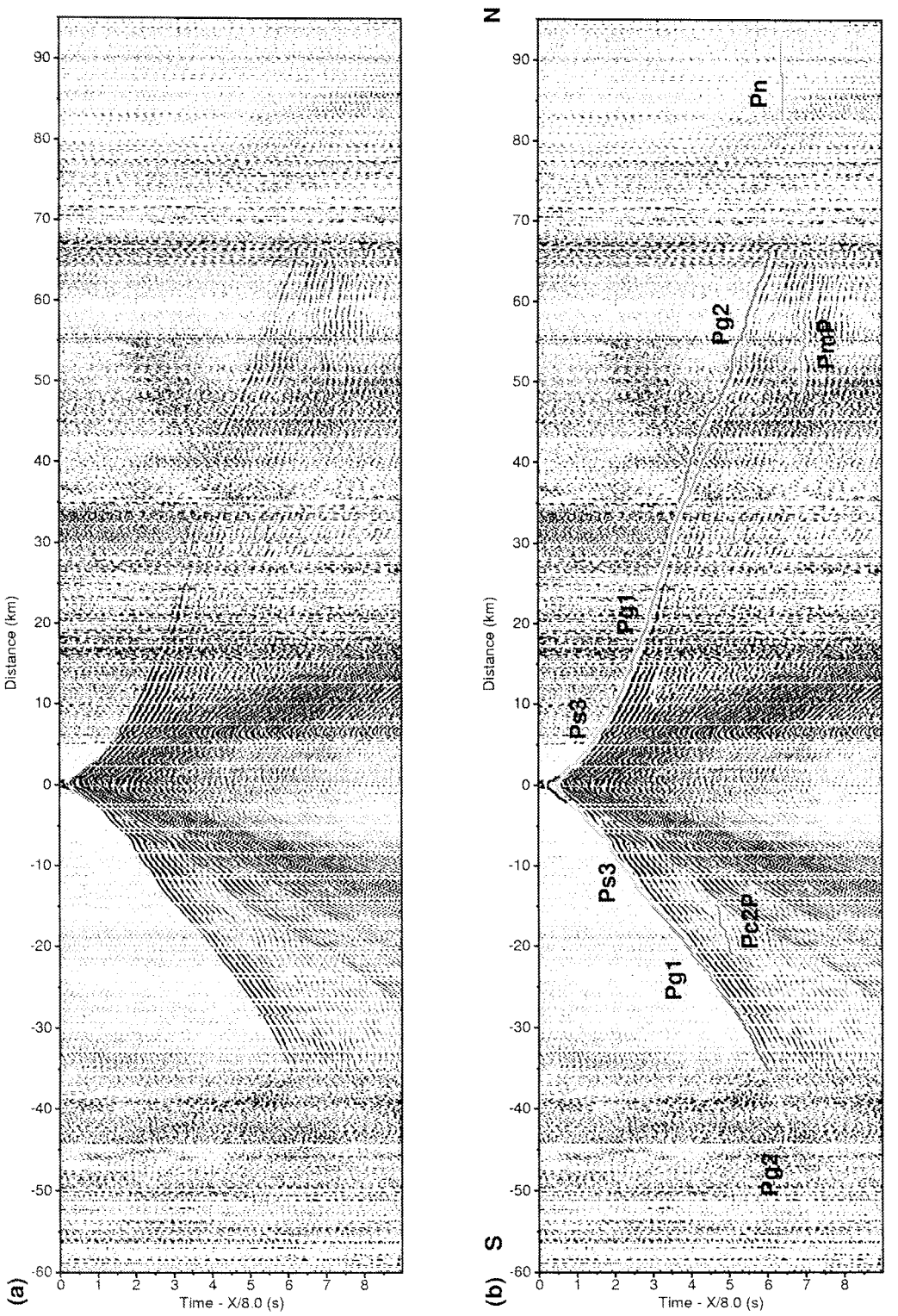

Figure 6. (a) Vertical component of the OBS data and (b) selected arrivals superimposed on the OBS data from station 6 on the top of the Ryukyu Arc slope. (c) Southern far-offset section with weak refracted arrival through the middle crust (Pg2), and (d) northern far-offset section with the refracted arrival through the upper mantle (Pn).

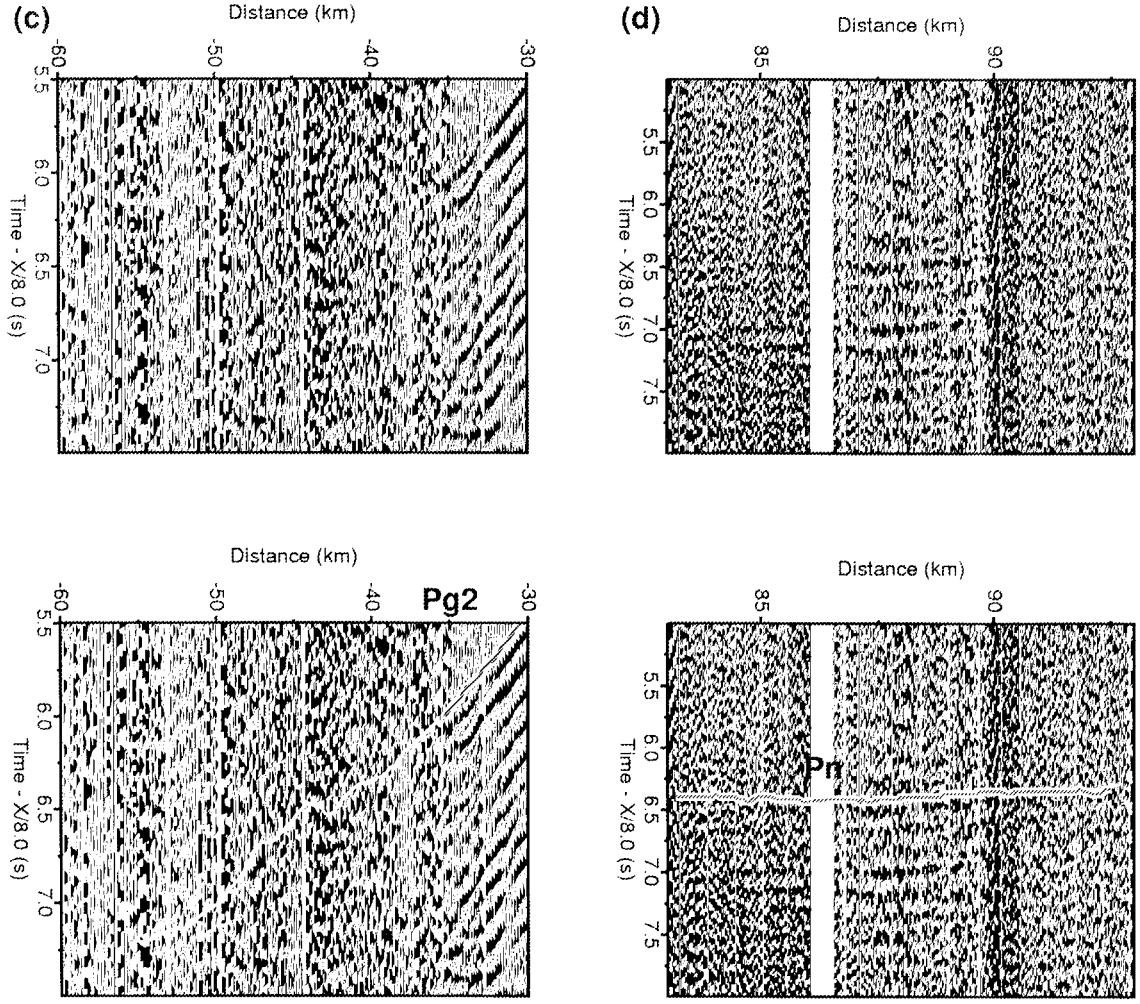

Figure 6. Continued.

At offsets greater than 10 km in OBS data at station 12 (Figure 2), refractions through the crust (Pg2 and Pg3), reflections from the Moho (PmP) and refractions through the upper mantle (Pn) provide good constraints for the velocity structure of the oceanic lithosphere below the Huatung Basin. In particular, the refractions from north of station 12 arrive much later than those from south of the station. This seems to indicate that the oceanic crust does not subduct until to the north of the station. However, since the maximum offset (70 km) of the identified arrivals (Figure 2) is much less than the corresponding maximum offset of the complete dataset listed in Table 1 (156.629 km for OBS 12), the upper-mantle structure further to the north of OBS station 12 cannot be well imaged from this OBS data.

Ryukyu Trench

Reflections and refractions through the sediment have been clearly identified at near offsets of $-20\sim20$ km from OBS 11 (Figure 3) in the Ryukyu Trench. Other arrivals, such as lower-crust refraction (Pg3), Moho reflection (PmP) and upper-mantle refraction (Pn) at far offsets, provide good constraints for the lower crust and the upper mantle beneath the trench. For example, a sudden decrease of the apparent velocity of the first arrivals (Pn) at 60 km south of OBS station 11 may indicate the beginning of the PSP subduction along EW9509-1. However, at offsets 35 km to 75 km, the OBS signals (white lines) are not strong enough for travel-time inversion. These weak signals will be discussed below.

Table 2. Nomenclatures of refracted and reflected phases.

	Refractions	Reflections
Upper sediment	Ps1	Ps1P
Lower sediment	Ps2	Ps2P
Compacted sediment	Ps3	Ps3P
Accretionary wedge		
Upper crust	Pg1	Pc1P
Middle crust	Pg2	Pc2P
Lower crust	Pg3	PmP
Upper mantle	Pn	

Yaeyama Ridge

The characteristics of the OBS data from stations 9 (Figure 4) and 10 located on the Yaeyama Ridge are quite different from those recorded by the OBS stations located in the Huatung Basin (Figure 2) and in the trench (Figure 3). First, early arrivals with low apparent velocities, identified as refractions through the accretionary prism (Ps3), extend further away from offsets −35 km to 20 km (Figure 4). Reflected arrivals from the base of the accretionary wedge (Ps3P) are also observed as later arrivals behind Ps3. Due to the long offset of these refracted and reflected arrivals, the structure of the thick prism can be well constrained below this station. Second, the apparent velocities of the first arrivals (Pg2 and Pg3) at the northern offsets seem to be higher, which may imply either high velocities or dipping interfaces. On the other hand, for deep events at the southern far-offset of OBS 9, only upper-mantle refraction (Pn) has been identified.

Forearc Basin

High apparent velocities of the earlier refracted arrivals from OBS data at station 8, extending from the southern offset of 35 km to the northern offset of 90 km, are observed on Figure 5. Since this station was located in the Nanao Forearc Basin, major sedimentary reflections (Ps1P and Ps2P) are readily observed. Two deeper reflections (Pc2P), one from the top of the subducting slab and the other from the intra-crustal interface of the Ryukyu Arc, are readily identified at offsets 10 km to 40 km in Figure 5. We also clearly observe PmP arrivals from the oceanic lithosphere at offsets −50 km to −20 km and from the continental lithosphere at offsets 60 km to 110 km.

Ryukyu Arc

OBS data and associated seismic phases of station 6 on the Ryukyu Arc slope are shown in Figures 6a and 6b. First and refracted arrivals are observed clearly at least from the southern offset of 35 km to the northern offset of 67.5 km. On the other hand, the refracted arrivals through the middle crust (Pg2) and the upper mantle (Pn) shown in Figure 6b can be readily identified in the enlarged sections of Figures 6c and 6d, respectively. Other reflected arrivals from the intra-crustal interface (Pc2P) and the Moho (PmP) are also observed (Figure 6b). The small number of reflected arrivals observed at the near offsets and at the early travel-time of this OBS data may imply thin or vanishing sediments on the Ryukyu Arc slope.

Layer-Stripping Inversion and Monte-Carlo Modeling

Instead of inverting all the parameters of a complicated model as suggested by Zelt (1999), we apply the layer-stripping inversion to construct a velocity-interface structure of EW9509-1, progressing gradually from the sediment to the crust. The reason for not employing simultaneous inversion of all the parameters is the difficulty of constructing an initial model for the subducting crust and of accommodating all the travel-time selections in advance. Layer-stripping inversion eliminates these difficulties because we only work one layer at a time. In this study, parameterization of uniform and dense grids was first applied to obtain the initial model, including the seafloor. Parameterization of non-uniform and sparse grids is subsequently achieved through modification of the initial model based on further inversion. Finally, when rays travel through the complex media such as pinch-out structures, the forward modeling is applied to correct the unrealistic results from inversion.

Inversion of sedimentary structures

Since refractions and reflections from sedimentary layers in the OBS data are concentrated only below the OBS stations, MCS data are required to better constrain sedimentary structures of the Huatung Basin, the Nanao Basin and the southern Okinawa Trough along EW9509-1. We first construct an initial model of the sedimentary layers based on the velocity analysis and the stacked section (e.g., Figure 7a) of the MCS data (Schnürle et al., 1998a). Layer-stripping inversion

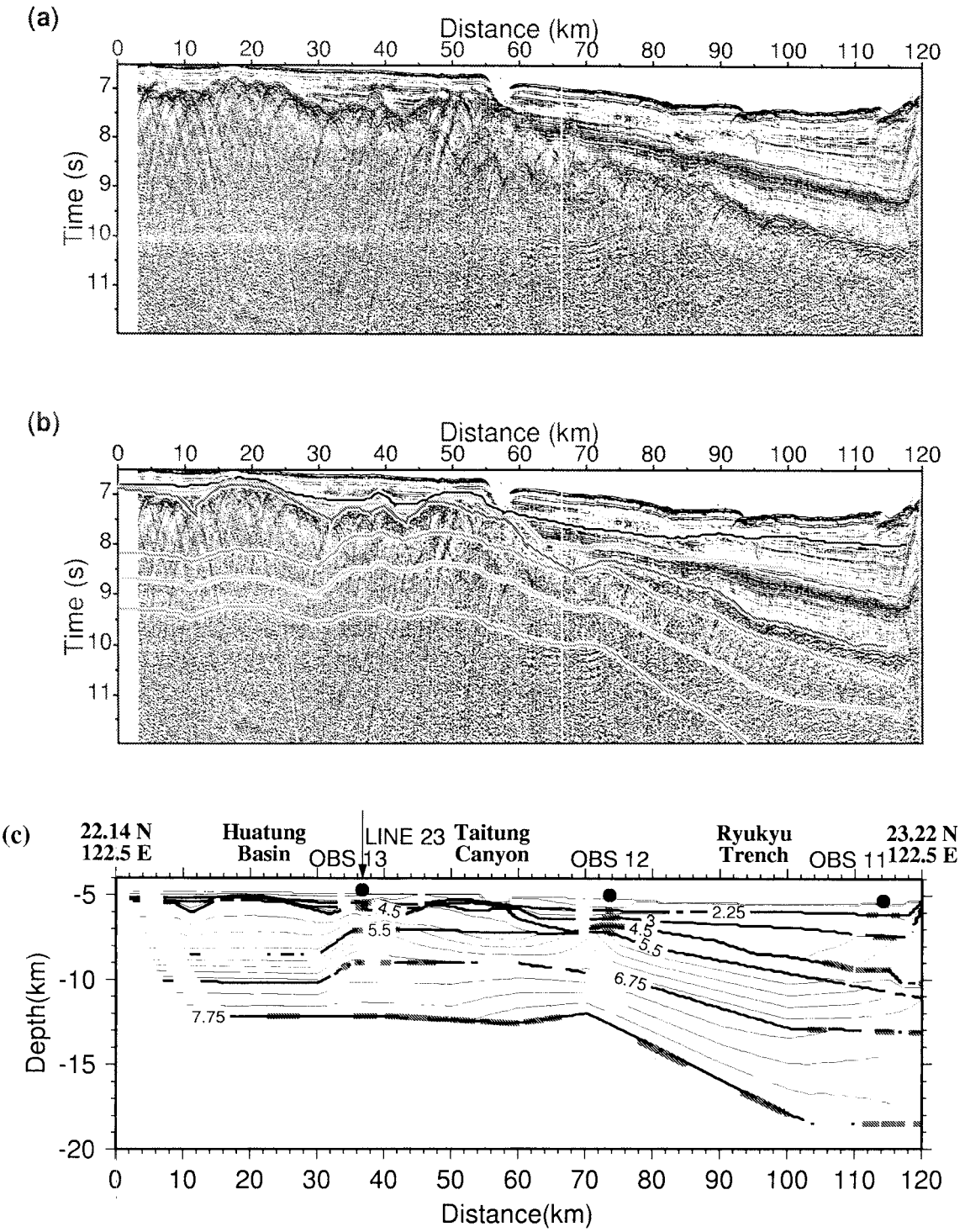

Figure 7. (a) Stacked MCS data along the southern portion of the EW9509-1 (in the Huatung Basin), (b) the calculated travel times (solid lines) superimposed on the stacked section and (c) the associated velocity-interface model developed in this study. The thick lines in (c) are reflection points from OBS data modeling. Velocity contours of 2.25, 3 and 4.5 km/s in (c), which correspond to three sedimentary layers in the Ryukyu Trench and the Huatung Basin, clearly match the reflecting signals in (a). Furthermore, PmP can be identified at least beginning at the Taitung Canyon and extending 15 km northward in (a).

(Zelt and Smith, 1992) of the sedimentary structures is then applied.

Inversion starts with refracted arrivals through the upper sediment (Ps1) in the OBS data. The uppermost refractions are employed to adjust the velocities within the layer (mainly the velocity of the upper part of the layer) until the root-mean-square (RMS) travel-time residual of the refraction from each station converges to its minimum level. The highest residual of the Ps1 is 70 ms at the northern offset of OBS 8, but no Ps1 arrival is picked from OBS 6 (Table 3). Inversion progresses to reflected arrivals from the bottom of the upper sediment to constrain the depth of the velocity interface. Two types of reflections, Ps1P arrivals from the OBS data and arrivals of normal incidence from the MCS data, are simultaneously used for inversion (Operto, 1996). In Table 3, the highest residual of the Ps1P is 85 ms at the southern offset of OBS 13, but no Ps1P arrival is observed from OBS 6 or the northern offset of OBS 9. Similarly, inversion continues downward to other sedimentary layers. To avoid breakdown of the travel-time inversion (Zelt and Smith, 1992) due to the fine grids and the complexity of the model, we also manually adjust grids of the model to obtain the minimum number of grids allowable based on the density of the rays. The highest travel-time residual in the sedimentary layers is 92 ms for refractions through the accretionary wedge south of OBS station 9, as indicated by the bold values in Table 3.

Along the southern portion of EW9509-1, the calculated arrivals from the OBS model are found to be consistent with the reflected signals in the stacked section (Figure 7b), and the reflection points of the OBS arrivals (the thick lines in Figure 7c) constrain the velocity interfaces of the model. This indicates that the bottoms of the upper, lower and compacted sediments in the Huatung Basin can be interpreted as velocity contours of 2.25, 3 and 4.5 km/s, respectively. Figure 7 also shows that the trench is about 60 km wide on EW9509-1. Furthermore, sedimentary interfaces are irregular south of the Taitung Canyon, while those in the Ryukyu Trench are uniform.

Inversion of crustal structures

Initial model building of the crustal structures can be accomplished through travel-time inversion of the first coherent arrivals (refraction) of the OBS data (generally known as transmission tomography). In particular, the dense velocity contours of the inverted model and the boundaries of different velocity gradients can be regarded as interfaces of the velocity discontinuities for further refining the initial model. Similar to the gradual downward inversion of the sedimentary structures, layer-stripping inversion of the crustal structures and the upper mantle starts from the upper-crust refraction (Pg1) and proceeds to the upper-crust reflection (Pc1P), the mid-crust refraction (Pg2), the mid-crust reflection (Pc2P), the lower-crust refraction (Pg3), the Moho reflection (PmP), and finally the upper-mantle refraction (Pn), as indicated in Table 3. In this study, the refracted arrivals and the reflected arrivals are generally applied to constrain the P-wave velocity and the depth of the velocity interface, respectively.

Monte-Carlo modeling

Since travel-time inversion (Zelt and Smith, 1992) of complex structures usually provides unrealistic results, diverges or even breaks down, a forward modeling is applied for fine-tuning the velocity-depth parameters. Similar to the Monte-Carlo method, we test one parameter at a time within a reasonable range to minimize the travel-time residuals and to maximize the ray coverage for correcting unrealistic parameters. The final results show that travel-time residuals greater than 90 ms are distributed mainly in the middle and lower crust (Pg2, Pg3 and PmP), as denoted by the bold values in Table 3. Except for the unavailable picks of the reflected arrivals in the Ryukyu Arc basement (north of OBS station 9), the forward modeling also enables us to identify the refracted and reflected arrivals to be as complete as possible. Therefore, Table 3 demonstrates the accuracy of the velocity and the interface from RMS travel-time residuals of refracted and reflected arrivals throughout the entire model, respectively.

Depth of the Moho beneath the Huatung Basin is found in the MCS data shown in Figures 7a and 7b, and the OBS velocity model shown in Figure 7c along the southern portion of EW9509-1. Deep reflections (PmP) are shown clearly at about 10 s TWT and at least 15 km northward from the Taitung Canyon in Figures 7a and 7b. By considering refracted arrivals from OBS stations 11, 12 and 13, most of the P-wave velocity of the oceanic crust (contours in Figure 7c) can be imaged. Reflected arrivals in the OBS data also constrain most of the Moho depths and the intracrustal interfaces (the thick lines in Figure 7c) beneath the OBS stations. Due to the interference of strong

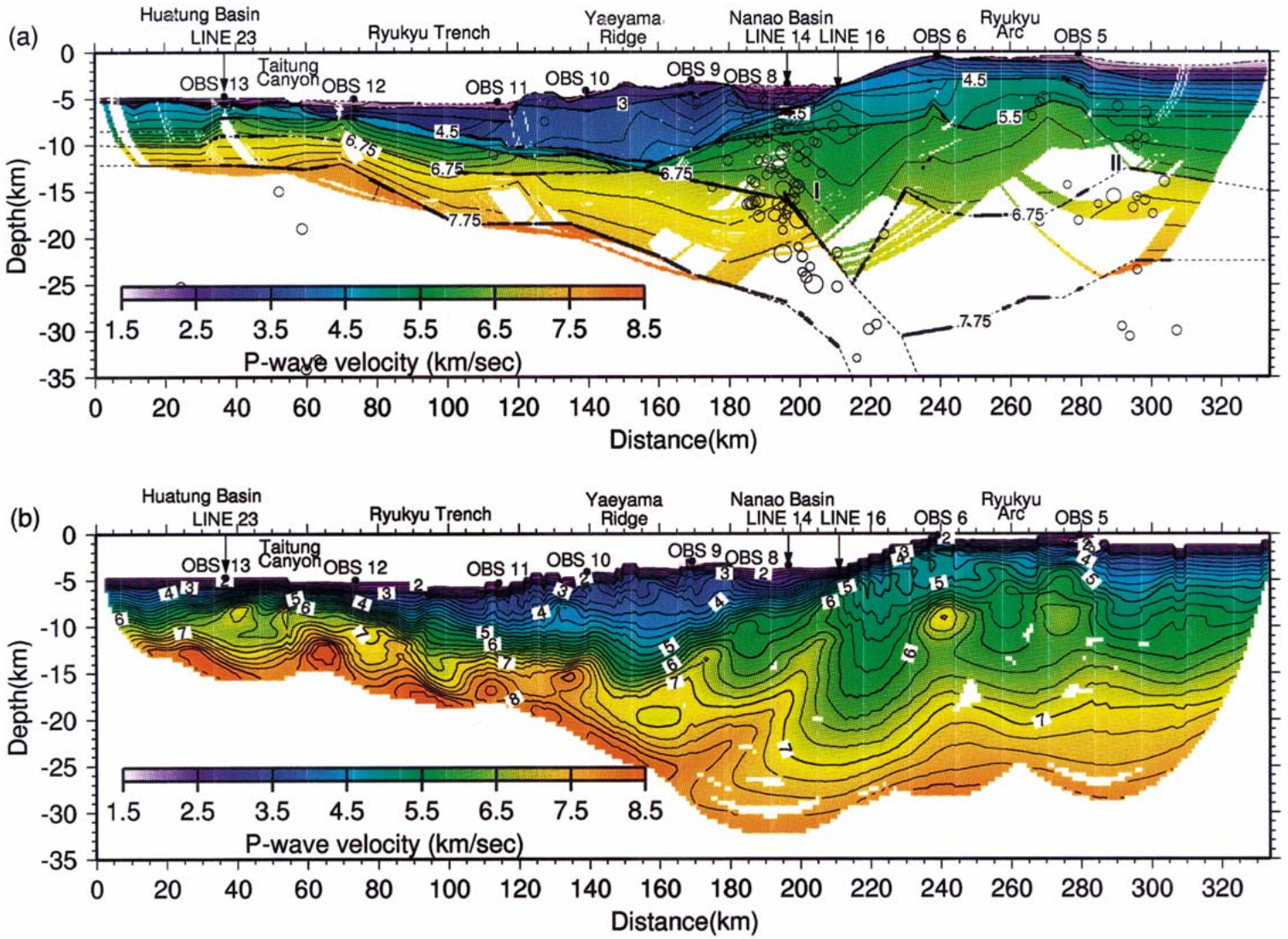

Figure 8. (a) A P-wave velocity-interface model (with coverage of refracted rays associated with apparent arrivals) along profile EW9509-1 in the southwestern Ryukyu subduction zone. The solid black lines are reflection points of the selected arrivals. The open circles are earthquake hypocenters (determined by the Central Weather Bureau, Taiwan) with magnitudes greater than 5, within 40 km of the profile and with errors of the epicenter and the focal depth less than 20 km. (b) A P-wave velocity model of EW9509-1 obtained using non-linear tomography with the refracted arrivals of the OBS data. The contour interval of both models is 0.25 km/s.

Table 3. RMS travel-time residual (ms) for each individual phase and station.

OBS Station	OBS 13		OBS 12		OBS 11		OBS 10		OBS 9		OBS 8		OBS 6		OBS 5	
Location(km)	36.68		73.572		114.199		139.323		169.288		196.568		239.064		279.384	
Offset																
Phase	S	N	S	N	S	N	S	N	S	N	S	N	S	N	S	N
Ps1	50	19	37	65	67	56	44	19	14	64	32	70	X	X	35	60
Ps1P	85	20	36	28	29	17	17	20	36	_	51	38	X	X	60	67
Ps2	_	_	_	_	74	36	78	34	37	_	45	48	30	45	X	X
Ps2P	_	_	12	21	49	28	_	_	38	52	33	34	29	10	X	X
Ps3	_	_	_	_	62	_	55	**90**	**92**	72	62	27	62	52	72	69
Ps3P	50	_	74	52	52	34	52	50	46	_	_	_	_	_	_	_
Pg1	84	_	_	**90**	_	50	58	_	55	X	**92**	69	40	46	61	53
Pc1P	12	46	43	12	_	_	34	18	51	15	42	40	_	_	_	_
Pg2	70	83	77	70	49	59	29	25	32	68	**103**	**91**	**105**	68	87	56
Pc2P	_	40	_	_	_	28	56	25	57	45	29	67	_	_	74	_
Pg3	44	39	63	**94**	86	**102**	47	68	31	55	_	_ ‖	**97**	X	89	_	_
PmP	43	55	**96**	**93**	73	71	69	69	76	_	74	**106** ‖	67	_	68	_	_
Pn	19	55	62	87	**158**	88	72	_	89	_	76	X	X	**123**	X	X

'‖' marks the boundary of the southern oceanic crust and the northern continental crust. The symbols 'X' and '_' stand for unavailable picks due to pinch-out structures in the model and the weak signals in the OBS data, respectively.

multiples and scattering, MCS data along the northern portion of EW9509-1 are not presented in this paper.

Validity of the Velocity-Interface Model

Non-linear tomography and alternative models

A P-wave velocity-interface model generated through layer-stripping inversion and Monte-Carlo modeling of refracted and reflected arrivals is presented in Figure 8a. To validate the velocity-interface model, non-linear tomography using back-projection and regularized inversion (Zelt and Barton, 1998) of the first arrivals in the OBS data is applied to generate an alternative model (Figure 8b). The grid interval of the tomography is 0.5 km along the length and the depth of the model. The velocity contour of 4.5 km/s, indicating the base of the Yaeyama accretionary prism and the top of the Ryukyu Arc basement, in the tomographic result agrees well with that in the velocity-interface model. Similarly, the velocity contour of 6.75 km/s south of OBS 10 in the tomographic model (Figure 8b) is consistent with an intra-crustal interface of the PSP in Figure 8a. Furthermore, the thickness of the subducting slab and the overriding plate (P-wave velocities of 4.5∼7.75 km/s) in both models is also very similar. However, the velocity contour of 6.75 km/s below the Nanao Basin in the tomographic model seems to be more undulated than that in the velocity-interface model. To test this difference, an initial model with an undulated interface below the Nanao Basin is applied in layer-stripping inversion. The inversion result shows contradictory reflected arrivals from OBSs 6, 8, and 9 (reflection points in Figure 8a) since non-linear tomography cannot constrain the structural interfaces through the reflected arrivals. Therefore, we prefer the result of layer-stripping inversion and Monte-Carlo modeling, which provides both reliable velocity and interface (Figure 8a).

Ray coverage

Since the weak arrivals (the white lines in Figures 3 to 6) of the OBS data are identified by comparing with the calculated arrivals from the velocity-interface model, they are not used in inversion but are employed only to demonstrate ray coverage. Furthermore, the final result (Figure 8a) is derived not only from inversion but also from forward modeling. Therefore, instead of using the resolution generated through inversion (Zelt and Smith, 1992), we present the ray coverage to validate the model. Refracted rays shown in Figure 9a cover most of the model at depths less than 25 km, but only a few rays travel through the lower crust and the upper mantle of the overlying plate

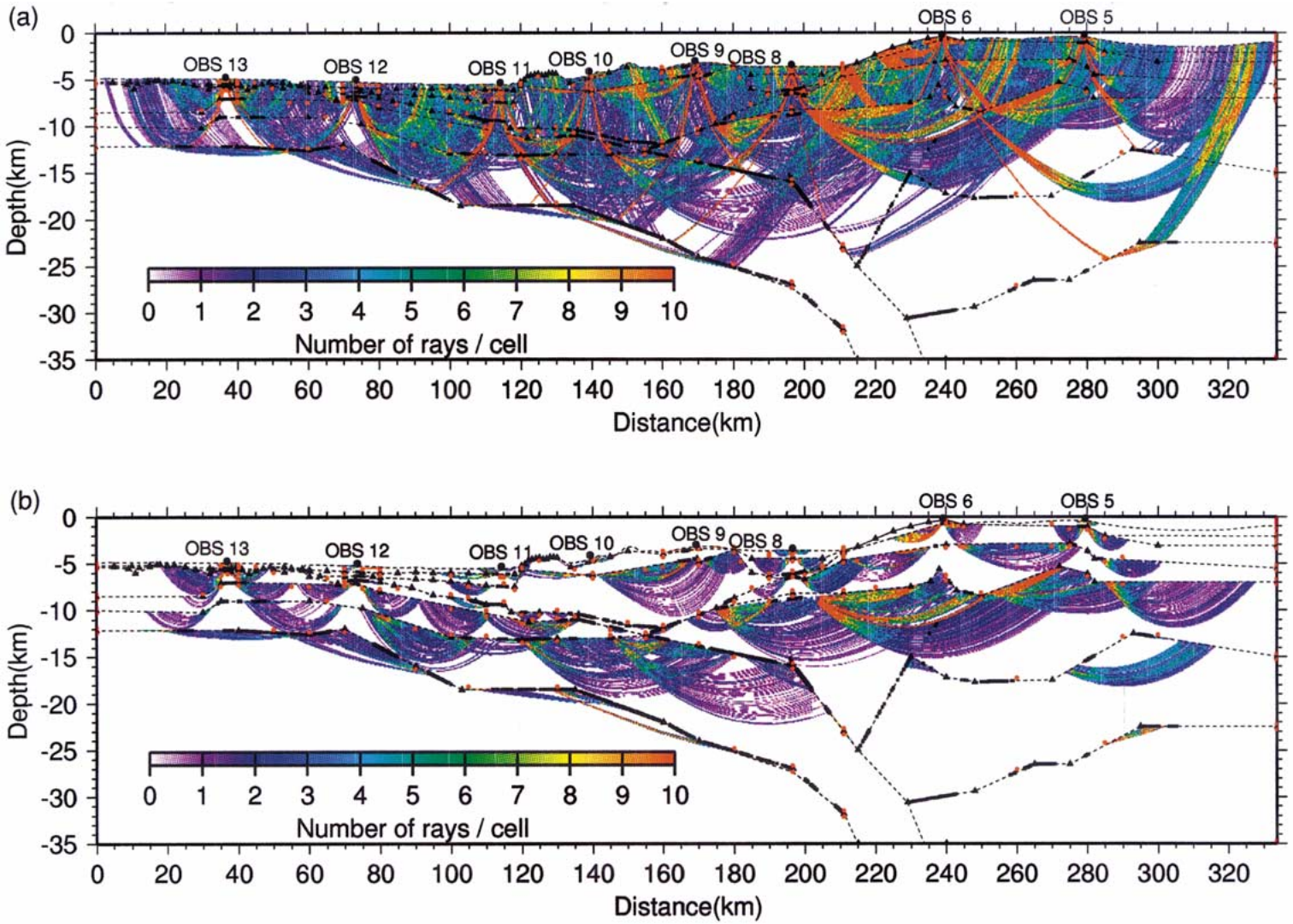

Figure 9. The number of refracted rays in each cell (color shaded) with both apparent and weak arrivals through (a) all layers and (b) their lowest layer along profile EW9509-1. The size of the cell for accounting the number of rays is 0.25 km and 0.05 km along the length and the depth of the model, respectively. Velocity grids (red circles), interface grids (black triangles) and reflection points of the selected arrivals (solid black lines) are also displayed to validate the velocity-interface model.

(Pg3 and Pn from OBSs 5, 6 and 8). The velocity structures of the sediment and the upper crust of the Ryukyu Arc are resolved best because the number of refracted rays in each cell exceeds 10. In view of the reflection points (the solid black lines) shown in Figure 9a, most of the interfaces of the velocity model are well constrained except for the intra-crustal interfaces beneath the Ryukyu Trench (Pc1P and Pc2P from OBSs 11 and 12) and the sedimentary layers above the Ryukyu Arc basement (Ps1P, Ps2P and Ps3P from OBSs 5 and 6). Moho is well imaged along EW9509-1 because there are sufficient coherent PmP and Pn arrivals as shown by the reflection points and refracted rays in Figure 9a, respectively.

The reason for displaying refracted rays through their lowest layer (Figure 9b) is that only the velocity within the lowest layer can be inverted from refracted arrivals when the model parameters of the upper (or previous) layers are fixed in the layer-stripping approach. Hence, we use the refracted rays through the lowest layer to confirm the proper distribution of the model parameters. The numbers of refracted rays in each cell (Figure 9b) are generally consistent with the velocity control points (the red circles) except for the sedimentary layers, which have additional constraints from the velocity analysis of the MCS data. The numbers of upper and lower velocity grids are, respectively, about 25 and 16 (or the average numbers of upper and lower grids are two and three below each station, respectively) in the compacted sediment and in the upper and middle crusts. Therefore, every refracted ray-group from each OBS station in their lowest layer is generally constrained by a trapezoidal model of the velocity grids (Zelt and Smith, 1992). Similarly, the reflection points of the selected arrivals (the solid black lines in Figure 9b) generally match the interface grids (the black triangles) except for the sedimentary layers, which have additional constraints from the reflected signals of the stacked MCS data. The maximum number of grids for an interface is 23 (or the average number of interface grids is three below each station) at the bottom of the upper crust. Thus, every reflected ray-group from each OBS station constrains at most a straight segment of the interface. The proper distribution of the velocity grids and the interface grids described above indicates the minimum-parameter model (Zelt, 1999) of this study.

Synthetic seismograms

Synthetic seismograms obtained using staggered-grid pseudo-spectral simulation (Chen, 1996) of the OBS data are also presented in Figure 10. These simulations are limited to the acoustic approach because we would only like to demonstrate the validity of the P-wave velocity model. The synthetic seismogram of OBS data from station 12 (Figure 10a) supports the strong amplitude and the variation of the apparent velocity from Pn at offsets 40 km to 70 km, as well as the weak amplitude of the arrivals beyond 70 km north of the station (Figure 2). The former can be attributed to the Yaeyama accretionary wedge, and the latter may result from the subducting slab. Furthermore, the similarities between the OBS data and the synthetic seismogram not only are observed in the first arrivals, but also in the later arrivals (PmP and other reflections at the near offsets shown in Figure 2 and Figure 10a). Similarly, the staggered-grid pseudo-spectral simulation of OBS data from station 8 (Figure 10b) demonstrates the amplitude variation of all first arrivals and of the later arrivals south of OBS station 8. However, north of the station, later events in the synthetic seismogram (Figure 10b) are much clearer than those in the OBS data, except for the dipping events (Pc2P) at offsets 10 to 40 km (Figure 5). The difference may be due to either interference caused by reverberation and signal attenuation in the OBS data, or inaccurate deep structures (perhaps the lower crust) north of OBS station 8.

Results and Discussions

We shall describe below the velocity-interface model (Figure 8a) and address its associated tectonic implications, again from south to north.

Huatung Basin

The sedimentary layers in the Huatung Basin as suggested by the model along profile EW9509-1 are composed of upper (1.51∼2.25 km/s), lower (2.25∼3 km/s) and compacted (3∼4.5 km/s) sediments. South of the Taitung Canyon, the thickness of the upper and lower sediments are 0.2∼0.6 km and less than 0.25 km, respectively (Figure 7c). However, in the southernmost profile, the thickness of the compacted sediment varies from non-existence to 0.6 km and the thickness of the upper crust (4.5∼5.5 km/s) are about 3 km south of OBS station 13 to 1.5 km north of it. The sediments to the north of the Taitung Canyon

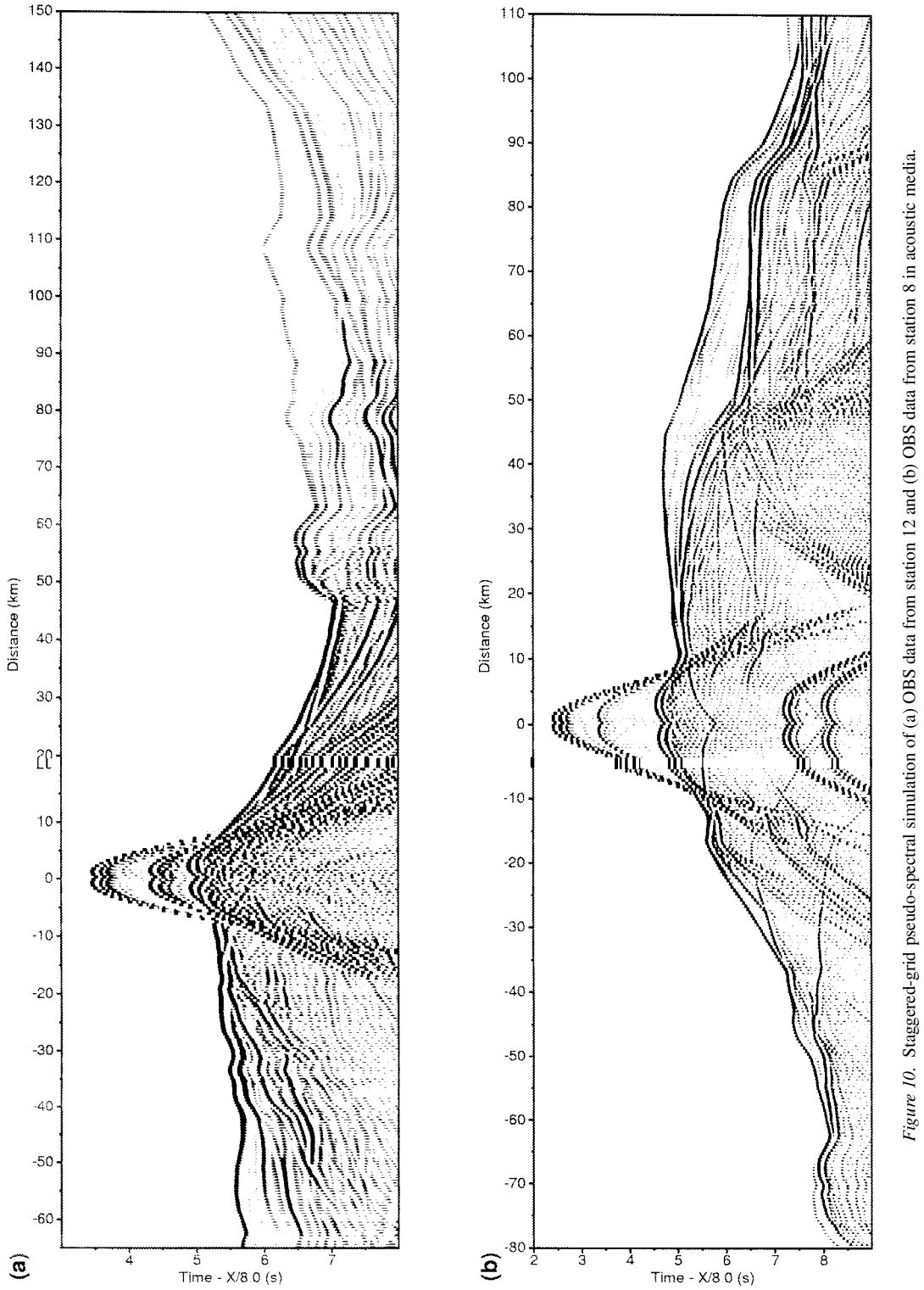

Figure 10. Staggered-grid pseudo-spectral simulation of (a) OBS data from station 12 and (b) OBS data from station 8 in acoustic media.

are less disturbed. The upper and lower sediments in the trench are 0.4∼0.6 km thick and from less than 0.5 km thick northward to about 1.3 km thick, respectively. The thickness of the compacted sediment in the Ryukyu Trench also increases from less than 0.5 km below the Taitung Canyon to about 2 km at the south end of the prism. The northward increase of sediment thickness in the trench reflects northward subduction of the PSP.

Yaeyama accretionary prism

North of the trench, a wedge-shape accretionary prism (3∼4.5 km/s) is developed (Figure 8a). The N-S extent of the accretionary wedge is about 75 km (model distance of 120∼195 km) and its average thickness is 4.5∼6.8 km. The base of the accretionary wedge reaches a depth of 11.9 km below the sea surface. The maximum thickness of the accretionary wedge is also similar to those in the middle (Kodaira et al., 1996) and northeastern (Iwasaki et al., 1990) Ryukyu subduction zones. The northern boundary of the wedge (or the backstop) starts beneath the Nanao Basin and extends southward at least 20 km with a dip of about 10 degrees. Undulation of the velocity contours within the northern part of the prism implies deformation of the prism due to compression with the Ryukyu Arc basement (backstop) and strike-slip faulting due to oblique convergence of the PSP (Lallemand et al., 1999).

Subducting slab of the PSP

North of about 160 km in the model distance in Figure 8a where the accretionary prism is the thickest, P-wave velocities in the upper part of the PSP are greater than 6.75 km/s. This may be attributed to the direct contact of the Ryukyu Arc basement with the PSP. Further northward below the Nanao Basin at distance of about 200 km in Figure 8a, the subducting angle of the oceanic crust increases abruptly northward from about 5 degrees between the Taitung Canyon and the Nanao Basin to about 25 degrees to the north. This important finding is fully confirmed from reflection points (black lines in Figure 8a) at the top of the subducting crust and is also supported by an earthquake swam (I in Figure 8a). Similarly, based on a one-to-one scale of the velocity-interface model along EW9509-1 (Figure 11), the subducting angle of about 25 degrees beneath the northern part of the Nanao Basin is consistent with the majority of the nodal planes of the earthquake focal mechanisms (Kao et al., 1998) in the southwestern Ryukyu forearc region. The rapid increase of the subducting angle is also similar to that in the Cascadia subduction zone offshore northern California (Leitner et al., 1998), where the post-subduction deformation, thrust faulting and crust shortening are prevailing from compression. Furthermore, at the bottom of the subducting slab, the depth of the Moho increases from 12.2 km south of the Taitung Canyon to 27.4 km beneath the Nanao Basin. The variation of the Moho leads to a crustal thickening (11 km) south of the Nanao Basin and a possible crustal thinning (7 km) north of the Nanao Basin where constraints from refracted arrivals through the lower crust are lacked. Therefore, we propose that the increasing angle of subduction, the crustal thickening and the possible crustal thinning are all attributed to the forearc compression and a possible break-off of the subducting slab (Teng et al., 2000) below the Nanao Basin.

Ryukyu Arc basement

Undulation of the velocity contours within the upper and middle crusts (4.5∼6.75 km/s) of the Ryukyu Arc shown in Figure 8a is well imaged by the dense refracted rays (Figure 9). Within the Ryukyu Arc basement and underneath the Ryukyu Arc slope, an intra-crustal interface (at a velocity contour of 6.75 km/s) is also well constrained by the reflected arrivals (indicated by the thick solid lines in Figure 12). This velocity interface, with a length of about 16 km, dips southward with an angle of about 30 degrees and may extend upward to the irregular interface (at a velocity contour of 5.5 km/s) below OBS station 6. Beneath the Ryukyu Arc basement, the depth of the Moho is northward decreasing from 30.6 km to 22.5 km within a distance of 65 km. The undulation of the velocity contours (4.5∼6.75 km/s), the variation of the intra-crustal interfaces (at velocity contours of 5.5 and 6.75 km/s) and of the Moho depths within and below the Ryukyu Arc may have resulted from forearc compression between the prism and the arc to the south, and backarc extension of the southern Okinawa Trough to the north. Two swarms of earthquakes (I and II in Figure 8a) beneath the Nanao Basin and between the southern Okinawa Trough and the Ryukyu Arc are evidence of forearc compression and backarc extension, respectively. Active earthquakes and forearc compression beneath the Nanao Basin are also

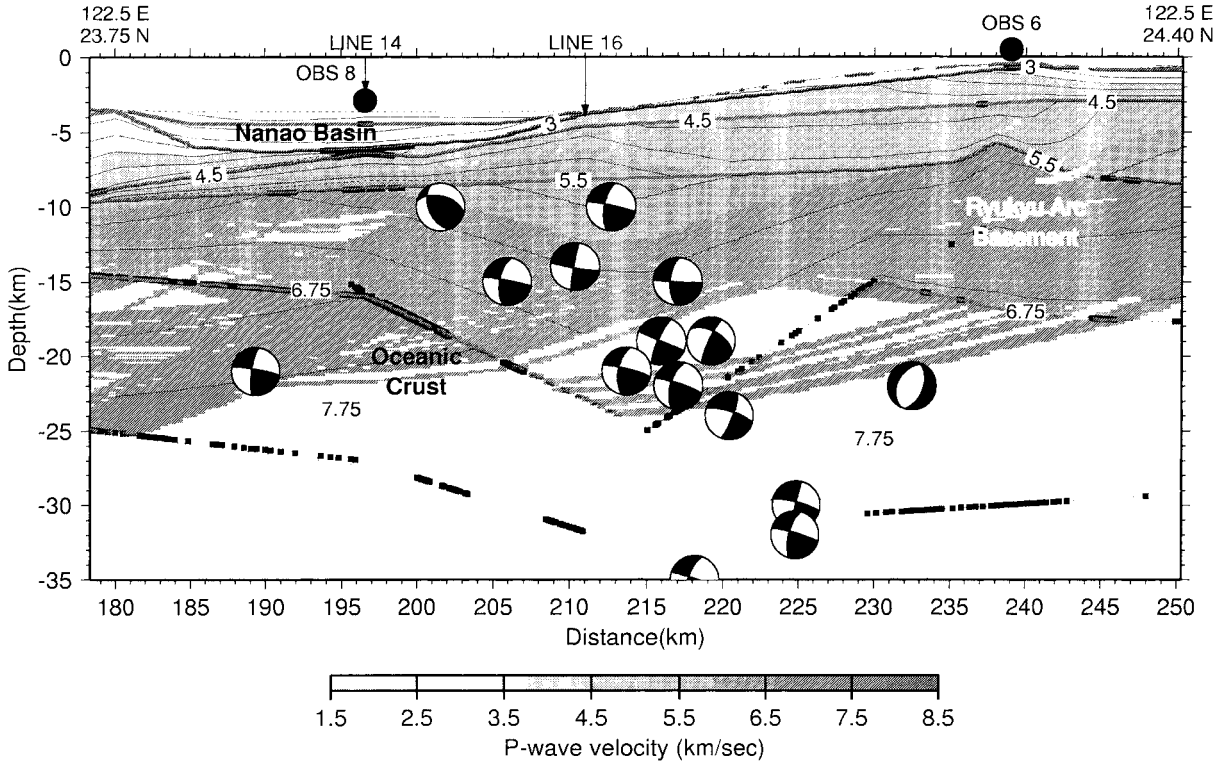

Figure 11. Sedimentary and crustal structures (1:1 scale) of the P-wave velocity and the focal mechanisms (Kao et al., 1998) along profile EW9509-1 in the southwestern Ryukyu forearc region. Focal spheres are projected onto the seismic profile and their darkened quadrants show the first motion of the compressional wave. Errors of the epicenter and the focal depth of these focal mechanisms are generally less than 5 km.

consistent with the predicted location of the tear fault (Lallemand et al., 1997).

We find similar velocity discontinuities in this study and in those of the middle (Kodaira et al., 1996) and northeastern (Iwasaki et al., 1990) Ryukyu subduction zones. Due to the limited ray coverage in the velocity-interface model, the lower crust and the upper mantle north of the Nanao Basin cannot be sufficiently imaged. Therefore, we cannot examine the hypotheses on the slab break-off (Teng et al., 2000) or the slab tear (Lallemand et al., 1997) in the upper mantle north of the Nanao Basin.

Conclusions

OBS data and MCS images across the southwestern Ryukyu subduction zone is presented in this paper. Layer-stripping inversion and Monte-Carlo modeling of refracted and reflected arrivals identified from the OBS/MCS data enables us to construct a velocity-interface model along profile EW9509-1. The final result is constructed based on the least travel-time residual of the individual phase and the consistency of the model grids and the number of rays. The former approach leads to good accuracy of the model, and the latter results in parameterization of the non-uniform and sparse grids. Except for the sedimentary layers above the Ryukyu Arc basement, all the upper (1.51∼2.25 km/s), lower (2.25∼3 km/s) and compacted (3.000∼4.50 kms/s) sediments along profile EW9509-1 are well imaged by the MCS and OBS data. Intra-crustal interfaces are well constrained at velocity contours of 5.5 km/s and 6.75 km/s, except below the Huatung Basin. Because there are sufficient, coherent PmP and Pn arrivals, Moho (7.75 km/s) is well constrained throughout the entire model.

North of the Taitung Canyon, the northward subduction of the PSP has resulted in a northward increase of the sedimentary thickness in the trench and a wedge-shaped Yaeyama accretionary prism north of the trench. The strongest compression due to subduction may have occurred below the Nanao Basin, as supported by earthquake hypocenters and focal mechanisms, leading to a sudden increase in the angle

of the subduction (from 5 degrees to 25 degrees), a sudden decrease in the thickness of the oceanic crust (from 11 km to 7 km) and a possible break-off of the slab beneath the Nanao Basin. The boundary between the subducting PSP and the Ryukyu Arc basement is found at a velocity contour of 6.75 km/s below the Nanao Basin. This boundary starts at a depth of 1 km below the thickest portion of the prism, continues to a depth of 13 km below the center of the Nanao Basin, and reaches a depth of 22 km below the toe of the Ryukyu Arc slope with a total length of about 62 km.

Forearc compression between the prism and the arc can be observed from the velocity undulation within the northern portion of the prism, while both forearc compression and backarc extension may have resulted in the observed velocity undulation and interface variation within the upper crust of the Ryukyu Arc. Two swarms of earthquakes beneath the Nanao Basin and between the southern Okinawa Trough and the Ryukyu Arc are evidence of forearc compression and backarc extension, respectively.

The velocity-interface structures established in this study reveal details of crustal deformation of this oblique subduction system in the southwestern Ryukyu Arc. Our velocity-interface model can be used in earthquake relocations and to provide additional constraints for determining focal mechanisms.

Acknowledgements

T. K. Wang would like to dedicate this work, his first international publication at NTOU, to the Lord. We thank S. Operto, G. L. Christeson and M. Wiederspahn for their helps at installation and usage of OBSTOOL, RAYINV and RSTTI. Figures except seismic images are generated from GMT (Wessel and Smith, 1995). Encouragements for writing up this manuscript from J.-C. Sibuet and C. S. Wang are appreciated. We thank two anonymous reviewers for their suggestions to improve this manuscript. Continuous funding supports from NSC 85-2611-M-019-003, NSC 86-2117-M-019-ODP, NSC 87-2611-M-002-A-016-ODP, NSC 88-2611-M-019-014-ODP are acknowledged.

References

Chen, H. W., 1996, Staggered-grid pseudospectral viscoacoustic wave field simulation in two-dimensional media, *J. Acous. Soc. Amer.* **100**, 120–131.

Christeson, G. L., 1995, OBSTOOL: software for processing UTIG OBS data, *University of Texas Institute for Geophysics, Technical Report*, No. 134, pp. 27.

Font, Y., Liu, C. S., Schnurle, P., and Lallemand, S., 2001, Constraints on backstop geometry of the southwest Ryukyu subduction based on reflection seismic data, *Tectonophysics* **333**, 135–158.

Hagen, R. A., Duennebier, F. K., and Hsu, V., 1988, A seismic refraction study of the crustal structure in the active seismic zone east of Taiwan, *J. Geophys. Res.* **93**, 4785–4796.

Henkart, P., 2000, SIOSEIS Users' Manual, Versions 2000.2, Scripps Institution of Oceanography, University of California.

Huang, C. Y., Yuan, P. B., Lin, C. W., Wang, T. K., and Chang, C. P., 2000, Geodynamic processes of Taiwan arc-continent collision and comparison with analogs in Timor, Papua New Guinea, Urals and Corsica, *Tectonophysics* **325**, 1–21.

Iwasaki, T., Hirata, N., Kanazawa, T., Melles, J., Suyehiro, K., Urabe, T., Moller, L., Makris, J., and Shimamura, H., 1990, Crustal and upper mantle structure in the Ryukyu Island Arc deduced from deep seismic sounding, *Geophys. J. Int.* **102**, 631–651.

Kao, H., Shen, S. S. J., and Ma, K. F., 1998, Transition from oblique subduction to collision: Earthquakes in the southernmost Ryukyu arc-Taiwan region, *J. Geophys. Res.* **103**, 7,211–7,229.

Kimura, M., 1985, Back-arc rifting in the Okinawa Trough, *Mar. Pet. Geol.* **2**, 222–240.

Kodaira, S., Iwasaki, T., Urabe, T., Kanazawa, T., Egloff, F., Makris, J., and Shimamura, H., 1996, Crustal structure across the middle Ryukyu trench obtained from ocean bottom seismographic data, *Tectonophysics* **263**, 39–60.

Lallemand, S. E., Liu, C. S., and Font, Y., 1997, A tear fault boundary between the Taiwan orogen and the Ryukyu subduction zone, *Tectonophysic* **274**, 171–190.

Lallemand, S. E., Liu, C. S., Dominguez, S., Schnürle, P., Malavieille, J., and the ACT Scientific Crew, 1999, Trench-parallel stretching and folding of forearc basins and lateral migration of the accretionary wedge in the southern Ryukyus: A case of strain partition caused by oblique convergence, *Tectonophysics* **18**, 231–247.

Leitner, B., Trehu, A. M., and Godfrey, N. J., 1998, Crustal structure of the northwestern Vizcaino block and Gorda Escarpment, offshore northern California, and implications for postsubduction deformation of a paleoaccretionary margin, *J. Geophys. Res.* **103**, 23,795–23,812.

Liu, C. S., Schnürle, P., Lallemand, S. E., and Reed, D. L., 1997, TAICRUST and deep seismic imaging of western end of Ryukyu arc-trench system, In K. Fujioka ed., Deep Sea Research in Subduction Zones, Spreading Centers and Backarc Basins, *JAMSTEC J. Deep Sea Res.*, 39–45.

Liu, C. S., Liu, S. Y., Lallemand, S. E., Lundberg, N., and Reed, D. L., 1998, Digital elevation model offshore Taiwan and its tectonic implications, *Terr. Atmo. Ocea.* **9**, 705–738.

McIntosh, K. D., and Nakamura, Y., 1998, Crustal structure beneath the Nanao forearc basin from TAICRUST MCS/OBS Line 14, *Terr. Atmo. Ocea.* **9**, 345–362.

Operto, S., 1996, RSTTI package: Ray Based Seismic Travel Time Inversion, *University of Texas Institute for Geophysics, Technical Report*, No. 148, pp. 36.

Schnürle, P., Liu, C. S., Lallemand, S. E., and Reed, D. L., 1998a, Structural insight into the south Ryukyu margin: Effects of the subducting Gagua Ridge, *Tectonophysics* **288**, 237–250.

Schnürle, P., Liu, C. S., Lallemand, S. E., and Reed, D. L., 1998b, Structural controls of the Taitung Canyon in the Huatung Basin east of Taiwan, *Terr. Atmo. Ocea.* **9**, 453–472.

Sibuet, J. C., Letouzey, J., Barbier, F., Charvet, J., Foucher, J. P., Hilde, T. W. C., Kimura, M., Chiao, L. Y., Marsset, B., Mullere, C., and Stephan, J. F., 1987, Back arc extension in the Okinawa Trough, *J. Geophys. Res.* **92**, 14,041–14,063.

Sibuet, J. C., and Hsu, S. K., 1997, Geodynamics of the Taiwan arc-arc collision, *Tectonophysics* **274**, 221–251.

Sibuet, J. C., Deffontaines, B., Hsu, S. K., Thareau, N., Le Formal, J. P., Liu, C. S., and the ACT party, 1998, Okinawa trough back-arc basin: Early tectonic and magmatic evolution, *J. Geophys. Res.* **103**, 30,245–30,267.

Teng, L. S., Lee, C. T., Tsai, Y. B., and Hsiao, L. Y., 2000, Slab breakoff as a mechanism for flipping of subduction polarity in Taiwan, *Geology* **28**, 155–158.

Wang, T. K., and Chiang, C. H., 1998, Imaging of arc-arc collision in the Ryukyu forearc region offshore Hualien from TAICRUST OBS Line 16, *Terr. Atmo. Ocea.* **9**, 329–344.

Wang, T. K., and Pan, C. H., 2001, Crustal Poisson's ratio off eastern Taiwan from OBS data modeling, *Terr. Atmo. Ocea.* (Suppl.), 249–268.

Wessel, P., and Smith, W. H. F., 1995, New version of the generic mapping tools (GMT) version 3.0 released, *Eos Trans. AGU* **76**, 329.

Yang, Y. S., and Wang, T. K., 1998, Crustal velocity variation of the western Philippine Sea Plate from TAICRUST OBS/MCS Line 23, *Terr. Atmo. Ocea.* **9**, 379–393.

Zelt, C. A., 1999, Modelling strategies and model assessment for wide-angle seismic traveltime data, *Geophys. J. Int.* **139**, 183–204.

Zelt, C. A., and Barton, P. J., 1998, Three-dimensional seismic refraction tomography: A comparison of two methods applied to data from the Faeroe Basin, *J. Geophys. Res.* **103**, 7187–7210.

Zelt, C. A., and Smith, R. B., 1992, Seismic traveltime inversion for 2-D crustal velocity structure, *Geophys. J. Int.* **108**, 16–34.